# Soluble endoglin antagonizes Met signaling in spindle carcinoma cells

Gaelle del Castillo, Esther Sánchez-Blanco, Ester Martín-Villar, Ana C. Valbuena-Diez[1], Carmen Langa[1] Eduardo Pérez-Gómez[Ψ], Jaime Renart, Carmelo Bernabéu[1] and Miguel Quintanilla[*].

Instituto de Investigaciones Biomédicas Alberto Sols, Consejo Superior de Investigaciones Científicas (CSIC)-Universidad Autónoma de Madrid (UAM), 28029-Madrid, Spain. [1]Centro de Investigaciones Biológicas, CSIC, and Centro de Investigación Biomédica en Red de Enfermedades Raras (CIBERER), 28040 Madrid, Spain.

[Ψ]Present address: Departamento de Bioquímica y Biología Molecular, Facultad de Biología, Universidad Complutense, 28040-Madrid, Spain.

*To whom correspondence should be addressed. Instituto de Investigaciones Biomédicas Alberto Sols, CSIC-UAM. Arturo Duperier 4, 28029-Madrid, Spain. Tel.: +34 91 5854412; Fax: +34 91 5854401; E-mail: mquintanilla@iib.uam.es

Running title: Soluble endoglin antagonizes Met

Key words: Soluble endoglin/TGF-β1/HGF/Met/MAPK/spindle cell carcinoma

Abbreviations: Eng, endoglin; Sol-Eng, soluble Eng, SCC, squamous cell carcinoma; SpCC, spindle cell carcinoma; HGF, hepatocyte growth factor; TGF-β1, transforming growth factor-β1; MAPK, mitogen-activated protein kinase; ERK, extracellular signal-regulated kinase.

**Abstract**

Increased levels of soluble endoglin (Sol-Eng) correlate with poor outcome in human cancer. We have previously shown that shedding of membrane endoglin, and concomitant release of Sol-Eng is a late event in chemical mouse skin carcinogenesis associated with the development of undifferentiated spindle cell carcinomas (SpCCs). In this report, we show that mouse skin SpCCs exhibit a high expression of hepatocyte growth factor (HGF) and an elevated ratio of its active tyrosine kinase receptor Met *vs* total Met levels. We have evaluated the effect of Sol-Eng in spindle carcinoma cells by transfection of a cDNA encoding most of the endoglin ectodomain or by using purified recombinant Sol-Eng. We found that Sol-Eng inhibited both mitogen-activated protein kinase (MAPK) activity and cell growth *in vitro* and *in vivo*. Sol-Eng also blocked MAPK activation by transforming growth factor-β1 (TGF-β1) and impaired both basal and HGF-induced activation of Met and downstream MAPK. Moreover, Sol-Eng strongly reduced basal and HGF-stimulated spindle cell migration and invasion. Both Sol-Eng and full-length endoglin were shown to interact with Met by coimmunoprecipitation experiments. However, full-length endoglin expressed at the plasma membrane of spindle carcinoma cells had no effect on Met signaling activity, and was unable to inhibit HGF-induced cell migration/invasion. These results point to a paradoxical suppressor role for Sol-Eng in carcinogenesis.

**Summary**

The ectodomain of the TGF-β coreceptor endoglin (CD105) is shed into the circulation and is called soluble endoglin (Sol-Eng). Here, we show that Sol-Eng blocks Met signaling activity and stimulation of spindle carcinoma cell migration/invasion by its ligand HGF.

## Introduction

Many cell-surface membrane receptors are proteolitically cleaved at their juxtamembrane region in a process called "shedding", which results in the release of the ectodomain into the extracellular space. Shedding may downregulate receptors at the cell surface and generate soluble forms that either antagonize or favor the formation of active signaling complexes with ligands (1). Endoglin (CD105) is a membrane glycoprotein that acts as a coreceptor for members of the transforming growth factor-β (TGF-β) superfamily, including TGF-β1, TGF-β3, activin-A, BMP2, BMP7, BMP9 and BMP10 (2). Endoglin plays a crucial role in cardiovascular development and angiogenesis (3, 4). Mutations in the endoglin gene are responsible for the hereditary hemorrhagic telangiectasia type 1 (HHT1), a vascular disorder characterized by epistaxis, cutaneous telangiectases and arteriovenous malformations in brain, lung and liver (5). In cancer, endoglin has also emerged as an important modulator of malignant progression by influencing tumor cell proliferation, motility, invasion and metastasis (reviewed in refs. 2, 6). Thus, endoglin behaves as a suppressor of malignancy in skin, esophageal, prostate and breast carcinomas (7-10), while promotes tumor growth and invasiveness in Ewing sarcoma and melanoma (11).

A soluble endoglin form (Sol-Eng) resulting from the cleavage of full-length endoglin by the membrane-anchored matrix metalloprotease MMP14 has been detected in the circulation associated with different pathologies, including preeclampsia and cancer (12-14). Preeclampsia is a specific syndrome of pregnancy characterized by hypertension and proteinuria, which is linked to elevated levels of Sol-Eng and placenta-derived soluble VEGF receptor 1 (also known as soluble fms-like tyrosine kinase-1, sFlt1) (15). Sol-Eng inhibits angiogenesis (12, 14) and increases blood pressure and vascular permeability (13, 14). Whereas it has been proposed that these

effects are mediated by Sol-Eng trapping circulating TGF-β1, thus impairing its binding to the functional receptors (14), other authors have found that Sol-Eng binds directly and with high affinity BMP9 and BMP10, but not TGF-β1 or TGF-β3 (16, 17). Sol-Eng has also been detected in the plasma, serum and urine of cancer patients. Interestingly, elevated levels of circulating Sol-Eng is a bad prognostic factor in breast, colorectal and prostate cancer that correlates with metastasis (18-21). We have shown that cleavage of membrane endoglin, and concomitant generation of Sol-Eng occurs during progression of chemical mouse skin carcinogenesis, which is associated with the development of highly malignant undifferentiated spindle cell carcinomas (SpCCs) (22). Though Hawinkels and coworkers suggested an anti-angiogenic role for Sol-Eng in the tumor microenvironment (12), the function of Sol-Eng in carcinogenesis remains to be determined.

Hepatocyte growth factor (HGF) signaling through its membrane tyrosine kinase receptor Met plays an important role during embryonic development and tissue remodeling. Yet, HGF/Met aberrant signaling is also associated with cancer, since Met hyperactivation promotes different processes related to malignant progression, including tumor cell proliferation, migration, invasion, metastasis and angiogenesis (23, 24).

In this work, we show that mouse spindle cell carcinomas generated by chemical carcinogenesis express elevated levels of HGF. Sol-Eng, but not membrane-bound full-length endoglin, inhibited baseline and HGF stimulated Met signaling, impairing proliferation, migration and invasion of spindle carcinoma cells. These results suggest an anti-oncogenic role for Sol-Eng in carcinogenesis.

## Materials and methods

*Cell culture conditions and treatments*

The origin and characteristics of the mouse epidermal cell lines used in this work are summarized in Supplementary Table 1 (available at *Carcinogenesis* Online). MCA3D and PB cells were kindly provided by Dr. S. Yuspa (National Cancer Institute, Bethesda, USA); PDV cells by Dr. NE Fusenig (German Cancer Research Center, Heidelberg, Germany); HaCa4, MSC11A5, CarB and CarC cells by Dr. A. Balmain (University of California, San Francisco, USA). CarC, the cell line most profusely used in this work, was derived from a poorly differentiated mouse skin carcinoma induced by chemical carcinogenesis (25). CarC was tested by microsatellite marker polymorphism analysis and found free of any contaminating cell (26). Cells were grown in Ham's F12 medium supplemented with amino acids and vitamins (MCA3D, PB, PDV, HaCa4) or Dulbecco's modified Eagle's medium (CarB, CarC, MSC11A5), in 10% fetal bovine serum and antibiotics (2.5 μg/ml amphotericin B, 100 μg/ml ampicillin, 32 μg/ml gentamycin) (Gibco). Cultures were maintained on plastic at 37ºC in a 5% $CO_2$-humidified atmosphere.

For TGF-β1 and HGF treatments, recombinant human TGF-β1 and HGF (PreproTech EC) were added to CarC cell transfectants growing in the absence of serum at the indicated concentrations. Treatments with recombinant human Sol-Eng (rhSol-Eng) were performed by pre-incubating cells with the indicated concentrations of rhSol-Eng (R&D Systems) for 1 h.

*Plasmids and transfections*

The HA-tagged human endoglin cDNA in pDisplay (27) was used to derive by PCR a truncated endoglin construct encoding a soluble form encompassing the orphan domain and the ZP-N domain (amino acids 26-437). The 1.3-kb PCR product was cloned into pCRII-TOPO (Invitrogen) and the endoglin fragment was inserted into the *EcoRI* site of the pCAGGS plasmid under the control of a ubiquitous actin promoter resulting in the pCAGGS-Sol-Eng vector (13). The plasmid pSV2neo (Clontech) contains a neomycin resistance gene.

CarC cells were co-transfected with pCAGGS-Sol.Eng and pSV2neo vectors at a 10:1 ratio, as described (28). Briefly, 10 μg of plasmid DNA were mixed with 20 μg of Lipofectamin (Life Technologies, Inc.) in serum-free medium according to the protocol provided by the manufacturer. Positive clones were selected in the presence of 400 μg/ml of the antibiotic G418 and screened for the presence of soluble endoglin using a commercial ELISA kit (Quantikine Human Endoglin/CD105, R&D Systems). Two clones expressing/secreting substantial amounts of Sol-Eng (CSE1 and CSE3) were selected for further studies. Parallel transfections with pSV2neo alone yielded endoglin-negative mock transfectants. Pooled clones were used for biochemical and functional studies.

HEK-293T cells were transiently cotransfected with cDNAs encoding the full-length wild-type human c-Met in pBABE puro vector (Addgene plasmid 17493; see ref. 29) and a cDNA encoding either the full-length human endoglin or its whole extracellular domain (amino acids 26-586, including the orphan domain and ZP-N and ZP-C domains), both tagged with HA, in pDisplay, as previously described (30). Cells

were lysed 24 h after transfection and protein expression was determined by Western blotting and coimmunoprecipitation experiments.

Stable transfection of the cDNA encoding the full-length human L-endoglin isoform subcloned into the pcDNA3 expression vector was carried out as previously described (22). CarC-Eng cells expressing endoglin at the plasma membrane were selected using a FACS Vantage cell sorter (Becton Dickinson). CarC cells transfected with the empty vector (CarC-neo) were used as a control.

*Real-time quantitative RT-PCR analysis*

RNA from tissues and cell lines was obtained using the RNeasy kit (Qiagen). Quantitative reverse transcription-PCR analysis was performed using the iScript Reverse Transcription Supermix kit (BioRad) in a 7900HT Fast (Life Technologies) instrument. The ribosomal protein RPLPO was used as an internal control of RNA quality and amplification. Taqman probes for HGF (Mm01135193-m1) and Met (Mm01156972-m1) were from Life Technologies.

*Western blot and coimmunoprecipitation experiments*

For detection of proteins in Western blots, cells were lysed at 4ºC in modified RIPA buffer and a cocktail of protease (2 μg/ml aprotinin; 2 μg /ml leupeptin; 1 mM phenylmethylsulfonil fluoride) and phosphatase (1 mM sodium orthovanadate; 2 mM β-glycerophosphate; 0.2 mM sodium fluoride) inhibitors (Sigma-Aldrich). Proteins were separated by sodium dodecyl sulfate-polyacrilamide gel electrophoresis and then transferred to Immobilon-P membranes (Millipore). For immunodetection of proteins, the following antibodies were used: 12CA5 mAb (Roche Diagnostics) for HA-Sol-Eng; P4A4 mAb (Santa Cruz Biotechnology) for human full-length endoglin (7); the mAb 1D4 recognizing glyceraldehyde-3-phosphate dehydrogenase (GAPDH) was purchased

from Enzo Life Sciences AG; the Abs specific for p44/42 MAPK (ERK1/2) (#9102), phospho-p44/42 MAPK (Thr202/Tyr204) (#9101S), as well as a mAb specific for phospho-Met (Tyr1234/1235) (D26) (#3077), all were from Cell Signaling; a polyclonal Ab recognizing Met (sc-162) was from Santa Cruz Biotechnology Inc. Appropriate secondary Abs coupled to horseradish peroxidase were used. Peroxidase activity was developed using an enhanced chemiluminiscence kit as indicated by the manufacturer (Pierce).

For coimmunoprecipitation experiments, cells were lysed in IP buffer (50 mM Tris-HCl, pH 8.0, 150 mM NaCl, 5 mM EDTA, 0.5% NP40) with a cocktail of protease inhibitors. Tagged Sol-Eng and Met were immunoprecipitated using anti-HA mAb (Roche Diagnostics) and anti-Met Ab sc-162 (Santa Cruz Biotechnology Inc.), respectively.

*Cell growth, migration and invasion assays*

For growth assays, cells were plated in triplicate in a 24-wells/plate at a density of 30,000 cells/well and grown in the absence of serum (with or without TGF-β1) for the indicated times. The relative number of cells was determined by staining with crystal violet and spectrophotometric reading (560 nm) of the solubilized dye. For cell proliferation assays, cells were seeded in 96 wells/plate at a density of 10,000 cells/well and grown in the presence or absence of serum for the indicated times. Incorporation of 5-bromo-2'-deoxyuridine (BrdU) was determined by using the Cell Proliferation ELISA BrdU kit (Roche Diagnostic).

Transwell migration assays were performed using Transwell chambers with 8-μm-pore polycarbonate filters (Corning) coated or not with 30 μg of Matrigel (Becton Dickinson). Cells were seeded in the upper compartment ($4x10^4$ cells per well) in

medium without serum and allowed to transmigrate for 15 h at 37ºC using 10% FBS, in the presence or absence of 100 ng/ml HGF, as chemoattractant. Cells on the upper side of the Transwell were then removed and those on the underside were fixed with methanol and stained with 1 μg/ml solution of 4',6-diamino-2-phenylindol (DAPI). Cell migration was quantified by counting the number of cells that migrated through the inserts. Four-five different fields were counted using an Axiophot fluorescence microscope (Carl Zeiss).

*Chemical carcinogenesis and tumorigenicity assays*

All animal experiments were approved by the Animal Care and Use Committees of the CSIC and UAM. Mice were cared for following institutional guidelines for animal care and in accordance with the standards established in the National Institutes of Health Guide for the Care and Use of Laboratory Animals. Induction of mouse skin tumors by initiation with a single dose of 7,12-dimethylbenz(*a*)-anthracene (DMBA) and promotion with 12-*O*-tetradecanoylphorbol-13-acetate (TPA) for 15 weeks has been previously described (22). Tumors were histologically typed by H&E staining of paraffin sections as well as by RT-PCR analysis of the following differentiation/progression markers: i) loss of K1/K10 expression in squamous cell carcinomas (SCCs); ii) induction of SPARC during progression from papillomas to SCCs; and iii) accumulation of Snail1 transcripts in poorly differentiated SpCCs.

For tumorigenicity assays, 1-2x$10^6$ cells were i.d. injected into the two flanks of 8-10 weeks-old female athymic nude mice (Harlan). The size of tumors was calculated from caliper measurements of two orthogonal diameters at different times. Tumors were excised and immediately frozen in liquid nitrogen for Western blot analysis and real-time RT-PCR.

*Statistical analysis*

Data are presented as mean ± SEM. Significance was determined using the Student's *t* test. Differences were considered significant at $p < 0.05$.

**Results**

*Sol-Eng attenuates MAPK signaling activity and inhibits cell proliferation of spindle carcinoma cells*

CarC is a malignant spindle cell line derived from a mouse skin carcinoma induced by chemical carcinogenesis (25). CarC has proteolytically inactivated membrane endoglin at the cell surface and sheds low baseline levels of Sol-Eng (22). In order to ascertain whether the presence of high levels of Sol-Eng in the extracellular medium affects CarC behavior, these cells were stably transfected with a cDNA encoding human Sol-Eng tagged with hemagglutinin (HA). Two clones (CSE1 and CSE3) expressing/secreting substantial levels of Sol-Eng (Fig. 1A, B) were selected, and their growth properties compared with those of control cells transfected with an empty vector (mock). Both CSE1 and CSE3 cells showed a slight but significantly reduced basal proliferation with respect to mock cells in the presence of serum (Fig. 1C). As CarC secretes autocrine growth factors, we also studied the growth properties of the transfectants in the absence of serum. In this case, reduced growth of CSE1 and CSE3 *vs* mock cells was more evident (Fig. 1D). It can be argued that Sol-Eng while being synthesized inside CSE cells could interfere with the cell cycle machinery slowing down proliferation. In order to address this possibility, we incubated cells with a purified recombinant human Sol-Eng (rhSol-Eng) protein and found that it efficiently inhibited both mock and CSE cell growth (Fig. 1E).

A slight reduction of cell growth was also observed *in vivo* after injection of CarC cell transfectants into athymic nude mice. Tumors induced by CSE3 (and also CSE1 at the first two weeks post-injection) grew slower than those induced by mock cells (Fig. 2A). The basis for the different tumorigenic behavior of CSE1 and CSE3 is presently unknown since both clones express similar levels of Sol-Eng *in vitro* (Fig. 1A, B) and *in vivo* (Fig. 2B). CarC cells carry oncogenic mutations in the two alleles of the *H-Ras* gene (26, 31), and display a hyperactivated Ras/mitogen-activated protein kinase (MAPK) signaling pathway. Interestingly, CSE1 and CSE3 showed reduced levels of phospho-extracellular signal-regulated kinase (ERK)1/2 compared to mock cells both *in vitro* (Fig. 2C) and *in vivo* (Fig. 2D), whereas no variation was observed in the total ERK1/2 expression levels. *In vitro*, this reduction was more pronounced in CSE3 (Fig. 2C), which may account for the slightly weaker tumorigenic potential of CSE3 with respect to CSE1 (Fig. 2A).

*Sol-Eng blocks TGF-β1-induced cell growth*

In contrast to normal keratinocytes and SCC cells, spindle carcinoma cells are not only insensitive to the TGF-β1 growth inhibitory response, but their growth is stimulated by the cytokine (32). Accordingly, proliferation of mock cells was slightly increased by TGF-β1 in a dose-dependent manner (Fig. 3A). In contrast, this TGF-β1-dependent growth stimulation did not occur in CSE3 cells. Moreover, TGF-β1 at 1 ng/ml was able to activate the ERK1/2 pathway in mock but not in CSE3 cells (Fig. 3B). A similar inhibitory effect on the TGF-β1-dependent activation of ERK1/2 was seen in parental CarC cells pre-incubated with rhSol-Eng (Fig. 3C). These results indicate that Sol-Eng inhibits TGF-β1 stimulation of MAPK signaling activity in CarC spindle cells.

*Enhanced expression of HGF is a late event in mouse skin chemical carcinogenesis*

Next, we asked whether Sol-Eng could inhibit cell growth and MAPK signaling activity triggered by activation of tyrosine kinase receptors. In a search for growth factors expressed/secreted by transformed keratinocytes, we found that CarC cells express remarkably high levels of hepatocyte growth factor (HGF) mRNA compared to other keratinocyte cell lines such as premalignant keratinocytes (MCA3D and PB), SCC cells (PDV and HaCa4) and SpCC cell lines (CarB and MSC11A5) (Fig. 4A). As a matter of fact, increased levels of HGF transcripts are mainly associated with the spindle phenotype during *in vivo* mouse skin carcinogenesis (Fig. 4B). The transcript levels of the HGF receptor Met remain low in transformed keratinocyte cell lines, with the exception of MCA3D and MSC11A5 that express relatively high levels (Fig. 4C). *In vivo*, Met expression is increased in SCCs with respect to premalignant stages of carcinogenesis, but Met transcript levels appear to diminish in SpCCs (Fig. 4D). Interestingly, when the levels of total and phosphorylated Met proteins were analyzed in the cell lines, spindle carcinoma cells (CarB, CarC and MSC11A5) showed enhanced levels of activated *versus* total Met protein expression compared to the other cell lines, and CarC displayed the highest phospho-Met/Met ratio (Fig. 4E). However, Met polypeptides (both the 170-kDa single chain precursor and the 145-kDa product corresponding to the β-chain of the mature receptor) were clearly downregulated in CarC compared to the other cell lines (Fig. 4E). These results might indicate that an autocrine loop exists in CarC by which secreted HGF continuously activates Met on the cell surface inducing its degradation, and are consistent with reports showing Met internalization and degradation induced by HGF (33, 34).

*Sol-Eng inhibits basal and HGF-induced Met signaling activity and coimmunoprecipitates with Met*

Subsequently, we studied the effect of Sol-Eng on basal and HGF-mediated Met activation of CarC cells. As shown in Fig. 5A, CSE1 and specially CSE3 cells displayed reduced levels of baseline active phospho-Met compared to mock cells. This result is consistent with the decreased baseline phospho-ERK1,2 levels and weaker tumorigenicity observed in CSE1 and CSE3 cells (Fig. 2A and C). In addition, HGF-dependent activation of Met and its downstream effector ERK1/2 were blocked in both CSE1 and CSE3 cells that express/secrete Sol-Eng (Fig. 5B, C). In mock cells, HGF induced the downregulation of Met shortly after stimulation for 5-10 min (Fig. 5B, C). Interestingly, baseline Met levels in CSE1 and CSE3 were also reduced with respect to mock cells (Fig. 5A-C), suggesting that expression of Sol-Eng induces the downregulation of Met. Likewise, preincubation of CarC cells with increasing concentrations of rhSol-Eng inhibited stimulation of Met signaling activity by HGF and downregulated Met levels in a dose-dependent manner (Fig. 5D). We next studied whether full-length human endoglin (Eng) was able to inhibit HGF stimulation of Met signaling. As shown in Figure 5E, Eng stably expressed at the plasma membrane of CarC cells (22) was unable to inhibit HGF-induced phosphorylation of both Met and ERK1/2. Also, Met protein levels were not affected by expression of full-length endoglin, but were down-regulated upon stimulation with HGF, as expected (Fig. 5E).

In order to ascertain whether Sol-Eng interacts with Met, we performed coimmunoprecipitation analysis. To this end, HEK-293T cells were cotransfected with constructs encoding Sol-Eng tagged with HA and untagged Met. Immunoprecipitation with anti-Met antibody clearly coprecipitated HA-Sol-Eng (Fig. 5F, upper panel), whereas a weaker coprecipitation signal of Met with anti-HA-Sol-Eng was detected

(Fig. 5F, lower panel). We also cotransfected constructs encoding Met and either Sol-Eng or full-length Eng, both tagged with HA, in HEK-293T cells. Interestingly, Met immunoprecipitation coprecipitated both full-length and truncated soluble endoglin proteins (Fig. 5G).

*Sol-Eng impairs migration/invasion of spindle carcinoma cells*

CarC cells are highly migratory and invasive *in vitro* and *in vivo* (35, 36). Using Transwell migration assays, in which the filter was coated (invasion) or not (migration) with Matrigel, HGF was able to stimulate further CarC cell migration and invasion by ~1.5 and ~4 folds, respectively, (Fig. 6A, B). In order to test whether Sol-Eng and full-length Eng had some effect on this behavior, we compared the migratory/invasive abilities of CSE3 and CarC-Eng with that of the parental and control cells before and after HGF stimulation. Compared to mock cells, CSE3 showed strongly decreased basal migratory and invasive abilities and were refractory to HGF stimulation (Fig. 6C, D). In contrast, CarC-Eng cells exhibited a substantial reduction in their migratory capacities under basal conditions, and showed only a slight, but non-significant, decreased invasiveness (Fig. 6A, B). Interestingly, HGF clearly stimulated cell migration and invasion in CarC-Eng and parental/control cells (~2 and ~4 folds, respectively; Fig. 6A, B), indicating that whereas Sol-Eng does interfere with Met-mediated CarC pro-migratory and pro-invasive properties, full-length Eng does not. These results are in agreement with the respective abilities of Sol-Eng and full-length Eng to impair or not HGF-induced Met signaling activity (Fig. 5).

**Discussion**

Membrane endoglin is cleaved in the juxtamembrane region by MMP14 to release Sol-Eng into the circulation, and increased levels of Sol-Eng are linked to poor prognosis in human breast, colorectal and prostate cancers (reviewed in refs. 2, 6). In addition, we found that shedding of membrane endoglin leading to release of Sol-Eng is a hallmark of progression to highly aggressive SpCCs during chemical mouse skin carcinogenesis (22). In this work, we have studied the effect of Sol-Eng on the behavior of CarC, a highly tumorigenic and metastatic spindle carcinoma cell line (35) that has hyperactivated the MAPK signaling pathway due to the presence of two mutated H-Ras alleles (31, 37). We report that Sol-Eng clearly inhibits MAPK activity and CarC cell growth *in vitro*. Although Sol-Eng was able to inhibit MAPK signaling activity also *in vivo*, its effect on the growth of tumors induced by CarC in nude mice was less pronounced (Fig. 2A). This could be due to the undetermined actions of Sol-Eng on stromal cells that might compensate the direct growth inhibitory effect exerted by this molecule on tumor cells. In this regard, it is also worth emphasizing the active crosstalk between stromal and tumor cells by which stromal-dependent epithelial endoglin shedding constitutes a mechanism that may exert an environmental control of cell malignancy (38). We also show that Sol-Eng counteracts the mild stimulation of CarC cell proliferation as well as the further activation of MAPK signaling induced by TGF-β1. The mechanism for this blockade is uncertain since although it has been reported that Sol-Eng acts as a scavenger for TGF-β1 preventing its binding to the cell surface receptors (14), this has been questioned by other laboratories (16, 17). Notwithstanding, the most striking observation of the present report is the inhibitory effect exerted by Sol-Eng on the activation of the tyrosine kinase receptor Met by its ligand HGF. Moreover, Sol-Eng strongly inhibited basal and HGF-induced spindle carcinoma cell migration and

invasion (Fig. 6). Interestingly, this effect is specific for Sol-Eng as membrane-bound full-length Eng was unable to inhibit the activation of Met and its downstream mediator ERK1,2 as well as the stimulation of cell migration/invasion by HGF (Figs. 5E, 6A, 6B). Although full-length Eng significantly reduced basal spindle carcinoma cell migration, this effect could be due to the inhibition of TGF-β1/Smad3 pro-migratory signaling activity (22). It is well established that HGF induces the internalization of Met and its subsequent degradation in the lysosomal compartment (reviewed in ref. 34). The fact that both transfected and recombinant Sol-Eng were able to downregulate Met in the absence of HGF (Fig. 5B-D), suggests the possibility that Sol-Eng can bind Met on the surface of CarC cells and promote its internalization. A schematic model depicting the role of HGF-induced Met internalization on Met signaling and the hypothetical inhibitory effect exerted by Sol-Eng is presented in Supplementary Fig. 1. As a matter of fact, we show that Sol-Eng interacts with Met by coimmunoprecipitation experiments (Fig. 5F, G). Because Met can associate with different membrane proteins, including integrins, the hyaluronan receptor CD44 and plexins (23), the question whether Sol-Eng binds Met directly or indirectly remains to be investigated. Intriguingly, full-length endoglin while coimmunoprecipitating with Met (Fig. 5G) was unable to downmodulate it and prevent its signaling activity.

Spindle carcinoma cell lines exhibit a high ratio of active phosho-Met respect to total Met protein levels compared with cell lines corresponding to earlier stages of tumor progression (Fig. 4F). This is due to the fact that spindle carcinoma cells tend to express higher levels of HGF. Indeed, elevated expression of HGF appears to be a hallmark of malignant progression during mouse skin carcinogenesis *in vivo*, since HGF levels increase during progression from papillomas to SCCs and are further enhanced in SpCCs (Fig. 4B). High levels of HGF in the serum of breast cancer patients correlate

with shorter disease-free survival and increased metastasis in lymph nodes (39, 40). In this respect, skin spindle cell carcinomas (represented by the CarC cell line) resemble claudin-low, basal-type breast carcinomas (41), where Met activation is associated with high aggressiveness and poor patient outcome (42, 43).

In summary, our results suggest that Sol-Eng antagonizes Met signaling activity at advanced stages of carcinogenesis. These data together with the anti-angiogenic action ascribed to Sol-Eng (12, 14, 17) point to a malignancy suppressor role for this circulating form of endoglin. Paradoxically, the levels of Sol-Eng increase at later stages of carcinogenesis and correlate with bad prognosis in human epithelial cancer (2, 4). It could be argued that Sol-Eng cannot counteract the full malignant strength displayed in the tumor microenvironment at late stages of carcinogenesis. In addition, Sol-Eng might act by preventing the development of cancer in premalignant stages. Supporting this view there is epidemiological evidence indicating that preeclamptic women expressing elevated levels of placental Sol-Eng are protected against the development of different types of cancer, including breast carcinomas, in later life. Nonetheless, there are dissenting reports on this matter (reviewed in ref. 44). Further studies are necessary to understand the role of soluble endoglin on tumor initiation and progression.

**Acknowledgements**

We thank Dr. Antonio Díaz-López (*Instituto de Investigaciones Biomédicas Alberto Sols*, CSIC-UAM, Madrid, Spain) for his help with migration/invasion assays. We also thank Drs. Stuart Yuspa (National Cancer Institute, Bethesda, USA), Norbert Fusenig (German Cancer Research Center, Heidelberg, Germany) and Allan Balmain (University of California, San Francisco, USA) for providing us with mouse epidermal

cell lines. This work was supported by grants from the *Ministerio de Economía y Competitividad* (SAF2010-19152 and SAF2013-46183-R to MQ, and SAF2010-19222 and SAF2013-43421-R to CB), *Comunidad Autónoma de Madrid* (S2010/BMD-2359, SkinModel, to MQ). CIBERER is an initiative of the *Instituto de Salud Carlos III*. GdC was the recipient of a Juan de la Cierva postdoctoral research contract. EP-G and EM-V are the recipients of a postdoctoral research contract from the scientific foundation of *Asociación Española Contra el Cáncer* (AECC).

**References**

1. Arribas, J. *et al*. (2002) Protein ectodomain shedding. *Chem. Rev.*, **102**, 4627-37.
2. Bernabeu, C. *et al*. (2009) The emerging role of TGFbeta superfamily coreceptors in cancer. *Biochim. Biophys. Acta*, **1792**, 954-73.
3. ten Dijke, P. *et al*. (2008) Endoglin in angiogenesis and vascular diseases. *Angiogenesis*, **11**, 79-89.
4. López-Novoa, J.M. *et al*. (2010) The physiological role of endoglin in the cardiovascular system. *Am. J. Physiol. Heart Circ. Physiol*., **299**, H959-H974.
5. McAllister, K.A. *et al*. (1994) Genetic heterogeneity in hereditary haemorrhagic telangiectasia: possible correlation with clinical phenotype. *J. Med. Genet.*, **31**, 927-32.
6. Pérez-Gómez, E. *et al*. (2010) The role of the TGF-β coreceptor endoglin in cancer. *TheScientificWorldJOURNAL*, **10**, 2367-84.
7. Quintanilla, M. *et al*. (2003) Expression of the TGF-beta coreceptor endoglin in epidermal keratinocytes and its dual role in multistage mouse skin carcinogenesis. *Oncogene*, **22**, 5976-85.

8. Wong V.C.L. *et al*. (2008) Identification of an invasión and tumor suppressing gene, Endoglin (ENG), silenced by both epigenetic inactivation and allelic loss in esophageal squamous cell carcinoma. *Int. J. Cancer*, **123**, 2816-23.
9. Lakshman, M. *et al*. (2011) Endoglin suppresses human prostate cancer metastasis. *Clin. Exp. Metastasis*, **28**, 39-53.
10. Henry, L.A. *et al*. (2011) Endoglin expression in breast tumor cells suppresses invasion and metastasis and correlates with improved clinical outcome. *Oncogene*, **30**, 1046-58.
11. Pardali, E. *et al*. (2011) Critical role of endoglin in tumor cell plasticity of Ewing sarcoma and melanoma. *Oncogene*, **30**, 334-45
12. Hawinkels, L.J. *et al*. (2010) Matrix metalloproteinase-14 (MT1-MMP)-mediated endoglin shedding inhibits tumor angiogenesis. *Cancer Res.,* **70**, 4141-50.
13. Valbuena-Díez, A.C. *et al*. (2012) Oxysterol-induced soluble endoglin release and its involvement in hypertension. *Circulation*, **126**, 2612-24.
14. Venkatesha, S. *et al*. (2006) Soluble endoglin contributes to the pathogenesis of preeclampsia. Nat. Med., **12**, 642– 49.
15. Young, B.C. *et al*. (2010) Pathogenesis of preeclampsia. *Annu. Rev. Pathol.*, **5**, 173-92.
16. Castonguay, R. *et al*. (2011) Soluble endoglin specifically binds bone morphogenetic proteins 9 and 10 via its orphan domain, inhibits blood vessel formation, and suppresses tumor growth. *J. Biol. Chem.*, **286**, 30034-46.
17. Gregory, A.L. *et al*. (2014) The enigmatic role of endoglin in the placenta. *Placenta*, **35S**, S93-S99.

18. Li, C. *et al*. (2000) Plasma levels of soluble CD105 correlate with metastasis in patients with breast cancer. *Int. J. Cancer*, **89**, 122-6.

19. Takahashi, N. *et al*. (2001) Association of serum endoglin with metastasis in patients with colorectal, breast, and other solid tumors, and suppressive effect of chemotherapy on the serum endoglin. *Clin. Cancer Res.*, **7**, 524-32.

20. Li, C. *et al*. (2003) Both high intratumoral microvessel density determined using CD105 antibody and elevated plasma levels of CD105 in colorectal cancer patients correlate with poor prognosis. *Br. J. Cancer*, **88**, 1424-31.

21. Karam, J.A. *et al*. (2008) Use of preoperativeplasma endoglin for prediction of lymph node metastasisin patients with clinically localized prostate cancer. *Clin. Cancer Res.*,**14**, 1418-22.

22. Pérez-Gomez, E. *et al*. (2007) A role for endoglin as a suppressor of malignancy during mouse skin carcinogenesis. *Cancer Res.*, **67**, 10268-77.

23. Trusolino, L. *et al*. (2010) Met signaling: principles and functions in development, organ regeneration and cancer. *Nat. Rev. Mol. Cell. Biol*., **11**, 834-48.

24. Gherardi, E. *et al*. (2012) Targeting MET in cancer: rationale and progress. *Nat. Rev. Cancer.*, **12**, 89-103.

25. Bremner, R. *et al*. (1990) Genetic changes in skin tumor progression: correlation between presence of a mutant ras gene and loss of heterozygosity on mouse chromosome 7. *Cell*, **61,** 407-17.

26. Pons, M. *et al*. (2005) Chromosomal instability and phenotypic plasticity during the squamous-spindle carcinoma transition: association of a specific T(14;15) with malignant progression. *Oncogene*, **24**, 7608-18.

27. Guerrero-Esteo, M. *et al*. (2002) Extracellular and cytoplasmic domains of endoglin interact with the transforming growth factor-beta receptors I and II. *J. Biol. Chem.*, **277**, 29197-209.

28. Letamendia, A. *et al*. (1998) Role of endoglin in cellular responses to transforming growth factor-beta: a comparative study with betaglycan. *J. Biol. Chem.*, **273**, 33011–19.

29. Wrobel, C.N. *et al*. (2004) Autocrine CSF-1R activation promotes Src-dependent disruption of mammary epithelial architecture. *J. Cell Biol.*, **165**, 263-73.

30. Pérez-Gómez, E. *et al*. (2005) Characterization of murine S-endoglin isoform and its effect on tumor development. *Oncogene*, **24**, 4450-61.

31. Quintanilla, M. *et al*. (1991) Comparison of ras activation during epidermal carcinogenesis in vitro and in vivo. *Carcinogenesis*, **12**, 1875-81.

32. Haddow, S. *et al*. (1991) Loss of growth control by TGF-beta occurs at a late stage of mousen skin carcinogenesis and is independent of ras gene activation. *Oncogene*, **6**, 1465-70.

33. Hammond, D.E. *et al*. (2001) Down-regulation of MET, the receptor for hepatocyte growth factor. *Oncogene*, **20**, 2761-70.

34. Lefebvre, J. *et al*. (2012) Met degradation: more than one stone to shoot a receptor down. *FASEB J.*, **26**, 1387-99.

35. Díaz-Guerra, M. *et al*. (1992) Expression of simple epitelial cytokeratins in mouse epidermal keratinocytes harboring Harvey ras gene alterations. *Cancer Res.*, **52**, 680-87.

36. Santibáñez, J.F. *et al*. (1999) Urokinase expression and binding activity associated with the transforming growth factor beta1-induced migratory and

invasive phenotype of mouse epidermal keratinocytes. *J. Cell. Biochem.*, **74**, 61-73.

37. Santibánez, J.F. *et al*. (2010) The TGF-beta co-receptor endoglin modulates the expression and transforming potential of H-Ras. *Carcinogenesis*, **31**, 2145-54.
38. Tobar, N. *et al.* (2014) Soluble MMP14 produced by bone marrow-derived stromal cells sheds epithelial endoglin modulating the migratory properties of human breast cancer cells. *Carcinogenesis*, **35**, 1770-79.
39. Yamashita, J. *et al*. (1994) Immunoreactive hepatocyte growth factor is a strong and independent predictor of recurrence and survival in human breast cancer. *Cancer Res.*, **54**, 1630–33.
40. Taniguchi, T. *et al*. (1995) Serum concentrations of hepatocyte growth factor in breast cancer patients. *Clin. Cancer Res.*, **1**, 1031–34.
41. Wong, C.E. *et al*. (2013) Inflammation and Hras signaling control epithelial-mesenchymal transition during skin tumor progression. *Genes Dev.*, **27**, 670-82.
42. Ponzo, M.G. *et al*. (2009) Met induces mammary tumors with diverse histologies and is associated with poor outcome in human basal breast cancer. *Proc. Natl. Acad. Sci. USA*, **106**, 12903-08.
43. Gastaldi, S. *et al*. (2013) Met signaling regulates growth, repopulating potential and basal cell-fate commitment of mammary luminal progenitors: implications for basal-like breast cancer. *Oncogene*, **32**, 1428-40.
44. Gingery, A. *et al*. (2009) Placental ischemia and breast cancer risk after preeclampsia tying the knot. *Expert. Rev. Anticancer Ther.*, **9**, 671-81.

**Legends to Figures**

**Figure 1**. Sol-Eng inhibits CarC cell proliferation. CarC cells were transfected with a cDNA encoding Sol-Eng tagged with HA. Two clones (CSE1 and CSE3) were selected for further studies. Pooled CarC cells transfected with the empty vector (mock) were used as a control. (**A**) Western blot analysis of HA-Sol-Eng protein levels expressed by the transfectants. (**B**) The levels of HA-Sol-Eng secreted by the cells into the conditioned media were determined by ELISA, as described in Materials and methods. (**C** and **D**) Cell growth assays in the presence (**C**) or absence (**D**) of serum. In **C**, ~10,000 cells were seeded and grown in medium plus 10% FBS. Proliferation was determined by incorporation of BrdU into DNA, as described in Materials and methods. In **D**, ~30,000 cells were seeded and grown in medium in the absence of serum. The relative number of cells was determined by crystal violet staining at the indicated times. Columns in **C** and **D** represent the average of triplicate determinations $\pm$ SEM, and values are represented as percentages with respect to mock (**C**) and time zero (**D**). (**E**) Cell proliferation assays measured by incorporation of BrdU into DNA of mock and CSE3 cells pre-incubated or not with purified rhSol-Eng (100 ng/ml). *p*-values were obtained using the Student's *t* test. $*p < 0.05$; $**p \leq 0.01$; $***p \leq 0.001$

**Figure 2.** Sol-Eng inhibits basal MAPK signaling activity in CarC cells and tumors. (**A**) Tumorigenic potential of mock and CSE cells. Cells were injected into the two flanks of athymic nude mice, and the size of tumors were measured periodically. The graph shows one representative experiment out of two independent ones. (**B**) The expression of HA-Sol-Eng was determined by Western blotting in two different tumors induced by each cell transfectant at 43 days post-injection. (**C** and **D**) Western blot analysis of ERK1/2 phosphorylation relative to the total expression levels in cell (**C**) and tumor (**D**) lysates. GAPDH was used as a loading control. Tumors analyzed were the same as in **B**.

**Figure 3.** Sol-Eng impairs TGF-β stimulation of CarC cell growth and MAPK signaling activity. (**A**) Cell growth assay in the presence of TGF-β1. Mock and CSE3 cells (~30,000) were seeded in culture dishes in the absence of serum and treated with the indicated concentrations of TGF-β1 for 48 h. Then, cell number was determined by crystal violet staining. Values are represented as percentages with respect to treatment with vehicle. *p*-values were obtained using the Student's *t* test. **p* < 0.05. (**B**) Western blot analysis of ERK1/2 phosphorylation relative to the total ERK1/2 expression levels of mock and CSE3 cells at different times of treatment with 1 ng/ml TGF-β1. (**C**) Western blot analysis of ERK1/2 phosphorylation relative to the total expression levels of ERK1/2 of CarC cells untreated and treated with 1 ng/ml TGF-β1 for 30 min, pre-incubated or not with purified rhSol-Eng (25 ng/ml) for 1 h. In **B** and **C**, GAPDH was used as a loading control.

**Figure 4.** HGF and Met expression during mouse skin carcinogenesis. (**A** and **B**) Transcriptional expression of HGF in mouse epidermal cell lines (**A**) and skin tumors induced by DMBA/TPA (**B**). (**C** and **D**) Transcriptional expression of Met in mouse epidermal cell lines (**C**) and skin tumors induced by DMBA/TPA (**D**). Normalized HGF and Met transcript levels were measured by real-time quantitative RT-PCR relative to RPLPO. Ep, normal epidermis; Pap, papilloma; SCC, squamous cell carcinoma; SpCC, spindle cell carcinoma; w, weeks. (**E**) Western blot analysis of Met phosphorylation relative to the total Met expression levels in mouse epidermal cell lines. Two different exposure times for Met are shown. Values indicated at the bottom represent the ratio of active Met *vs* total Met levels. The intensities of phospho-Met and Met bands in the blot were quantified by densitometric analysis and normalized to GAPDH, used as a control for protein loading.

**Figure 5.** Sol-Eng coimmunoprecipitates with Met and attenuates basal and HGF-induced Met signaling activity. (**A**) Western blot analysis of basal Met phosphorylation relative to the total Met expression levels in mock, CSE1 and CSE3 cells. (**B** and **C**) Western blot analysis of phospho-Met, Met, phospho-ERK1/2 and ERK1/2 in mock and CSE1 (**B**) or CSE3 (**C**) cells after stimulation with 20 ng/ml HGF for the indicated times. (**D**) Western blot analysis of phospho-Met, Met, phospho-ERK1/2, ERK1/2 in CarC cells untreated or treated with 20 ng/ml HGF for 5 min, pre-incubated with the indicated concentrations of purified rhSol-Eng for 1 h. The discontinuous line indicates that lanes fifth and sixth are not contiguous but belong to the same gel (see Supplementary Figure 6A, available at *Carcinogenesis* Online). (**E**) Western blot analysis of phospho-Met, Met, phospho-ERK1/2, ERK1/2 and endoglin (Eng) in CarC cells stably transfected with a cDNA encoding full-length endoglin (CarC-Eng) or the empty vector (CarC-neo) after stimulation with 20 ng/ml HGF for the indicated times. GAPDH was used as a loading control. (**F**) HEK293T cells were transiently cotransfected with Met and HA-tagged Sol-Eng. After 24 h of transfection, the indicated amounts of total lysates were immunoprecipitated with anti-Met Ab (upper panel), anti-HA mAb (lower panel) and rat IgG as a control. Immunopreciptates were subjected to SDS-PAGE electrophoresis and immunoblotted with anti-HA (upper panel) and anti-Met (lower panel) antibodies. The presence of Met and HA-Sol-Eng in the precipitates were determined with the corresponding antibodies. (**G**) HEK-293T cells were transiently cotransfected with untagged full-length, wild type c-Met and either full-length Eng (Eng) or Sol-Eng, both tagged with HA. After 24 h of transfection, total lysates were immunoprecipitated with anti-Met Ab or rabbit IgG as a control. Immunopreciptates were subjected to SDS-PAGE electrophoresis and immunoblotted

with anti-HA mAb. The presence of Met in the precipitate was determined with anti-Met Ab.

**Figure 6.** Sol-Eng but not full-length Eng inhibits stimulation of CarC cell migration and invasion by HGF. (**A** and **B**) Transwell migration assays through uncoated (**A**) and Matrigel-coated (**B**) filters of parental CarC, CarC-neo and CarC-Eng cells. (**C** and **D**) Transwell migration assays through uncoated (**C**) and Matrigel-coated (**D**) filters of mock and CSE3 cells. HGF (100 ng/ml) was used as a chemoattractant. Migrated cells on the underside of the filter were fixed, stained with DAPI and counted. Values are represented as percentages with respect to unstimulated CarC cells. *p*-values were obtained using the Student's *t* test. *$p < 0.05$; **$p \leq 0.01$; ***$p \leq 0.001$; ns, non-significant. Panels below the graphics show representative examples of migrated/invaded cells stained with DAPI.

**Supplementary Figure Legends**

**Supplementary Figure 1. Hypothetical model for the role of Sol-Eng on the HGF/Met/MAPK pathway**. (**A**) The binding of HGF to the extracellular region of Met induces its dimerization and subsequent autophosphorylation in several tyrosines located in the juxtamembrane domain, the kinase domain and the C-terminal docking site. Phosphorylation of Met leads to recruitment of adaptor proteins and activation of downstream signaling pathways, including MAPK, which induces biological responses. Phosphorylation of Met also induces clathrin-dependent internalization of the receptor via early endosomes and its subsequent degradation in lysosomes. Met endocytosis is not only required for Met degradation but also favors signal transduction (Lefebvre et al. 2012, FASEB J., 26, 1387-99). (**B**) When the levels of Sol-Eng are increased due to the proteolytic shedding of membrane endoglin (that may occur in tumor as well as in stromal cells), Sol-Eng binds Met preventing its dimerization and activation by HGF. The binding of Sol-Eng also induces Met degradation by an unknown mechanism, which might involve internalization and lysosomal degradation (as depicted in the figure for simplicity) or not. Whether Sol-Eng is co-internalized with Met remains to be determined.

**Supplementary Figure 2. Uncropped images corresponding to the immunoblots included in figures.** (**A**) Uncropped images of Western blots in Figure 1A. (**B**) Uncropped images of Western blots in Figure 2B. (**C**) Uncropped images of Western blots in Figure 2C.

**Supplementary Figure 3. Uncropped images corresponding to the immunoblots included in figures.** (**A**) Uncropped images of Western blots in Figure 2D. (**B**) Uncropped images of Western blots in Figure 3B.

**Supplementary Figure 4. Uncropped images corresponding to the immunoblots included in figures.** (**A**) Uncropped images of Western blots in Figure 3C. (**B**) Uncropped images of Western blots in Figure 4E. (**C**) Uncropped images of Western blots in Figure 5A.

**Supplementary Figure 5. Uncropped images corresponding to the immunoblots included in figures.** (**A**) Uncropped images of Western blots in Figure 5B. (**B**) Uncropped images of Western blots in Figure 5C.

**Supplementary Figure 6. Uncropped images corresponding to the immunoblots included in figures.** (**A**) Uncropped images of Western blots in Figure 5D. (**B**) Uncropped images of Western blots in Figure 5E.

**Supplementary Figure 7. Uncropped images corresponding to the immunoblots included in figures.** (**A**) Uncropped images of Western blots in Figure 5F, upper panel. (**B**) Uncropped images of Western blots in Figure 5F, lower panel. (**C**) Uncropped images of Western blots in Figure 5G.

**Figure 1**

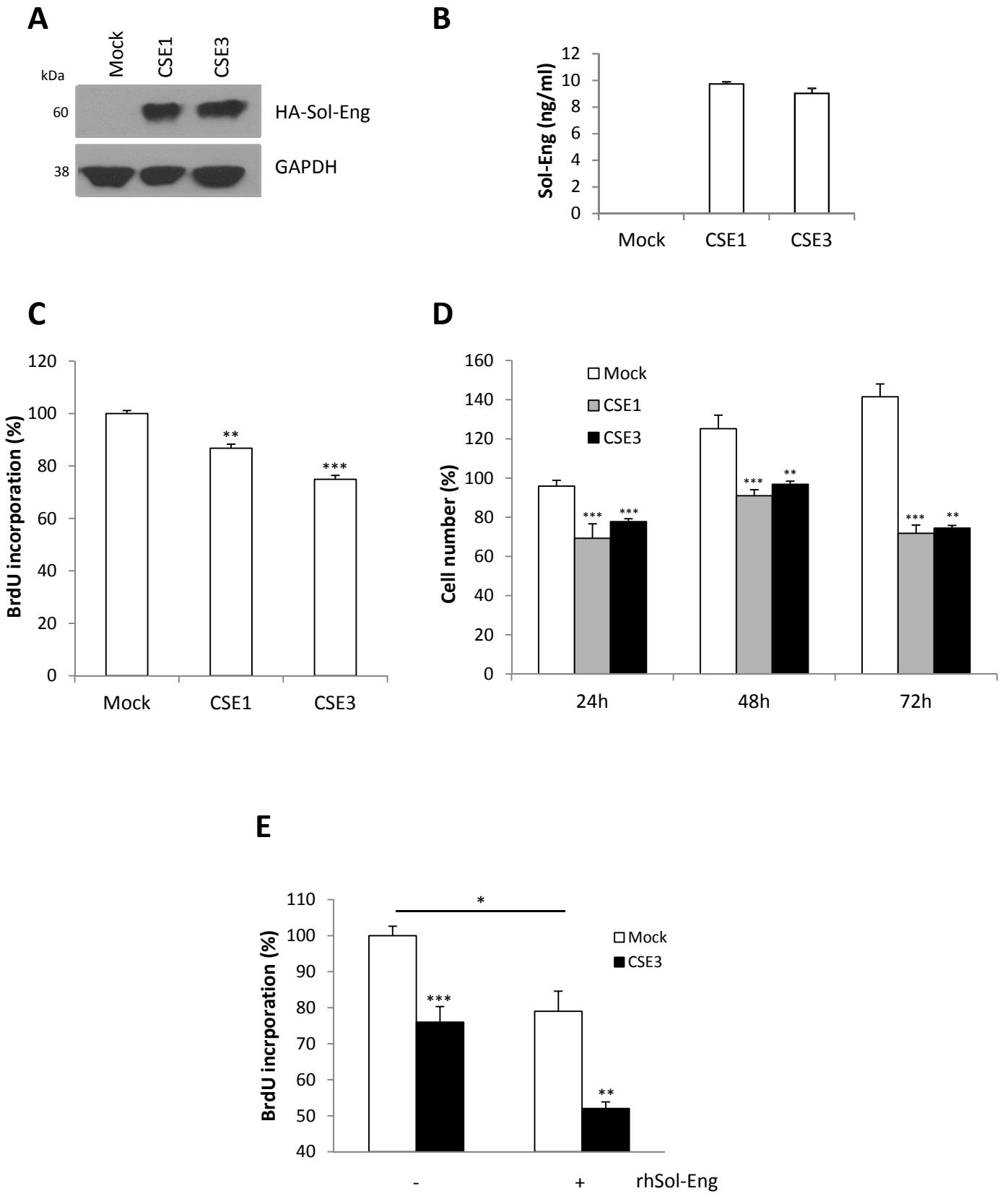
A
Mock
CSE1
CSE3
kDa
60
38
HA-Sol-Eng
GAPDH
B
Sol-Eng (ng/ml)
12
10
8
6
4
2
0
Mock
CSE1
CSE3
C
BrdU incorporation (%)
120
100
80
60
40
20
0
**
***
Mock
CSE1
CSE3
D
Cell number (%)
160
140
120
100
80
60
40
20
0
Mock
CSE1
CSE3
***
***
***
**
***
**
24h
48h
72h
E
BrdU incrporation (%)
110
100
90
80
70
60
50
40
*
***
**
Mock
CSE3
-
+
rhSol-Eng

# Figure 2

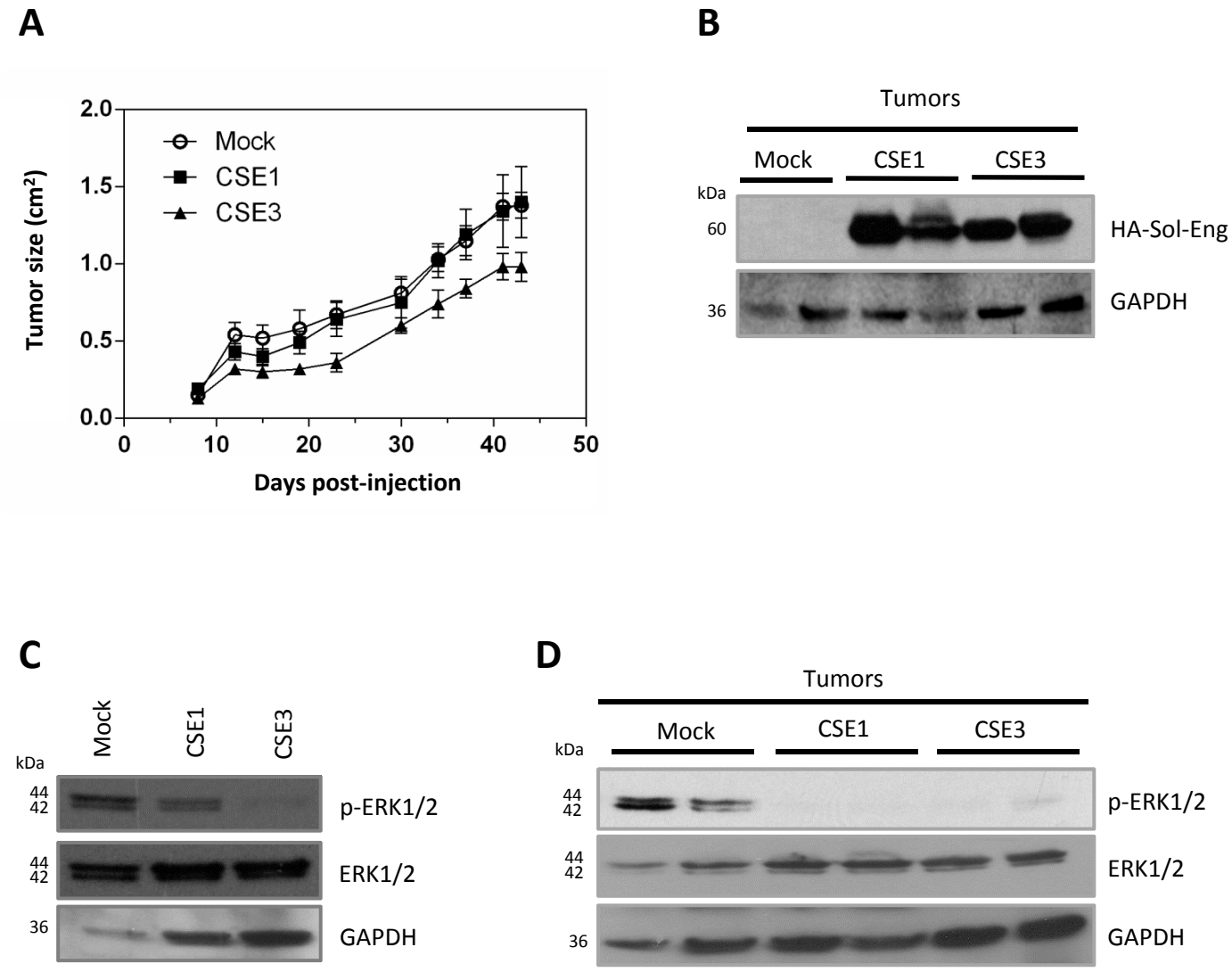
A
Tumor size (cm²)
2.0
1.5
1.0
0.5
0.0
0
10
20
30
40
50
Days post-injection
Mock
CSE1
CSE3
B
Tumors
Mock
CSE1
CSE3
kDa
60
HA-Sol-Eng
36
GAPDH
C
Mock
CSE1
CSE3
kDa
44
42
p-ERK1/2
44
42
ERK1/2
36
GAPDH
D
Tumors
Mock
CSE1
CSE3
kDa
44
42
p-ERK1/2
44
42
ERK1/2
36
GAPDH

**Figure 3**

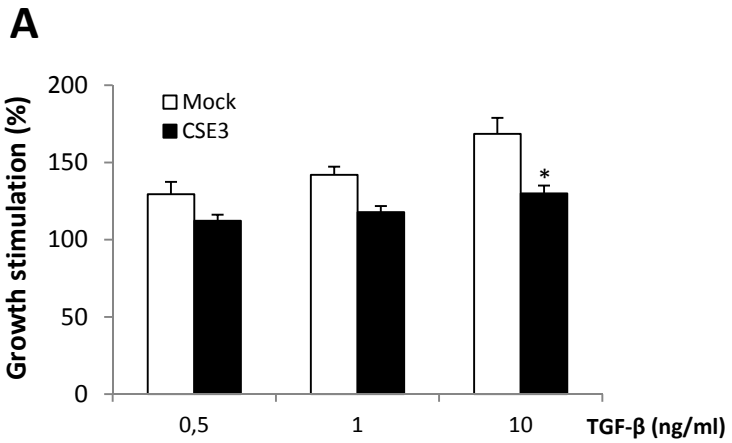
A
Growth stimulation (%)
200
150
100
50
0
Mock
CSE3
*
0,5
1
10
TGF-β (ng/ml)

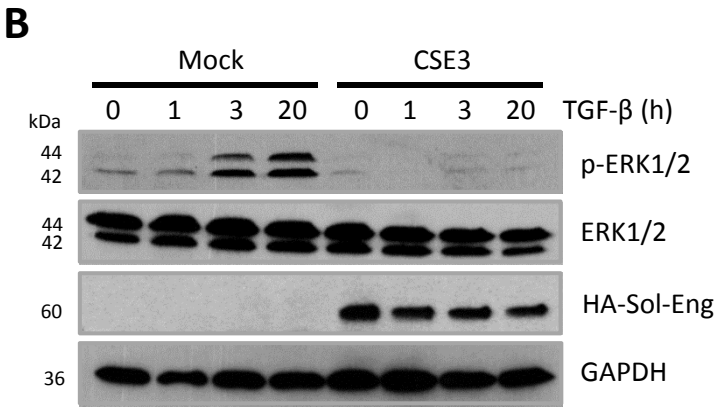
B
Mock
CSE3
kDa
0 1 3 20 0 1 3 20 TGF-β (h)
44
42
p-ERK1/2
44
42
ERK1/2
60
HA-Sol-Eng
36
GAPDH

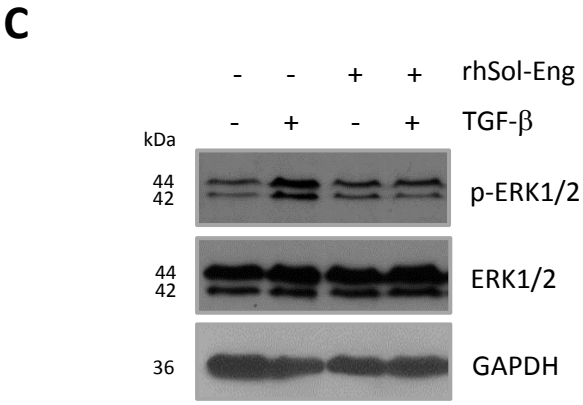
C
- - + + rhSol-Eng
- + - + TGF-β
kDa
44
42
p-ERK1/2
44
42
ERK1/2
36
GAPDH

**Figure 4**

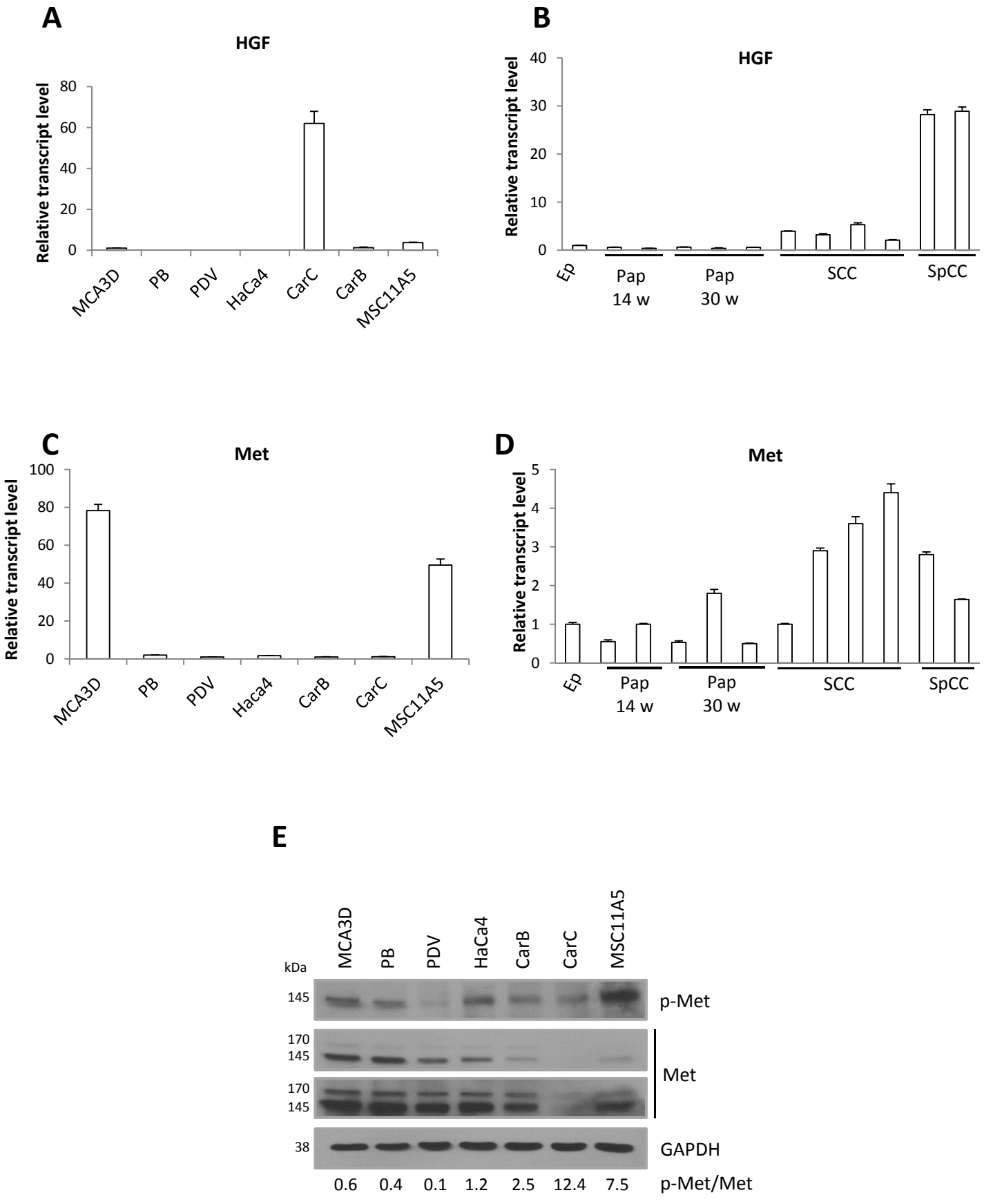
A
HGF
Relative transcript level
80
60
40
20
0
MCA3D
PB
PDV
HaCa4
CarC
CarB
MSC11A5
B
HGF
Relative transcript level
40
30
20
10
0
Ep
Pap 14 w
Pap 30 w
SCC
SpCC
C
Met
Relative transcript level
100
80
60
40
20
0
MCA3D
PB
PDV
Haca4
CarB
CarC
MSC11A5
D
Met
Relative transcript level
5
4
3
2
1
0
Ep
Pap 14 w
Pap 30 w
SCC
SpCC
E
kDa
MCA3D
PB
PDV
HaCa4
CarB
CarC
MSC11A5
145
p-Met
170
145
170
145
Met
38
GAPDH
0.6
0.4
0.1
1.2
2.5
12.4
7.5
p-Met/Met

# Figure 5

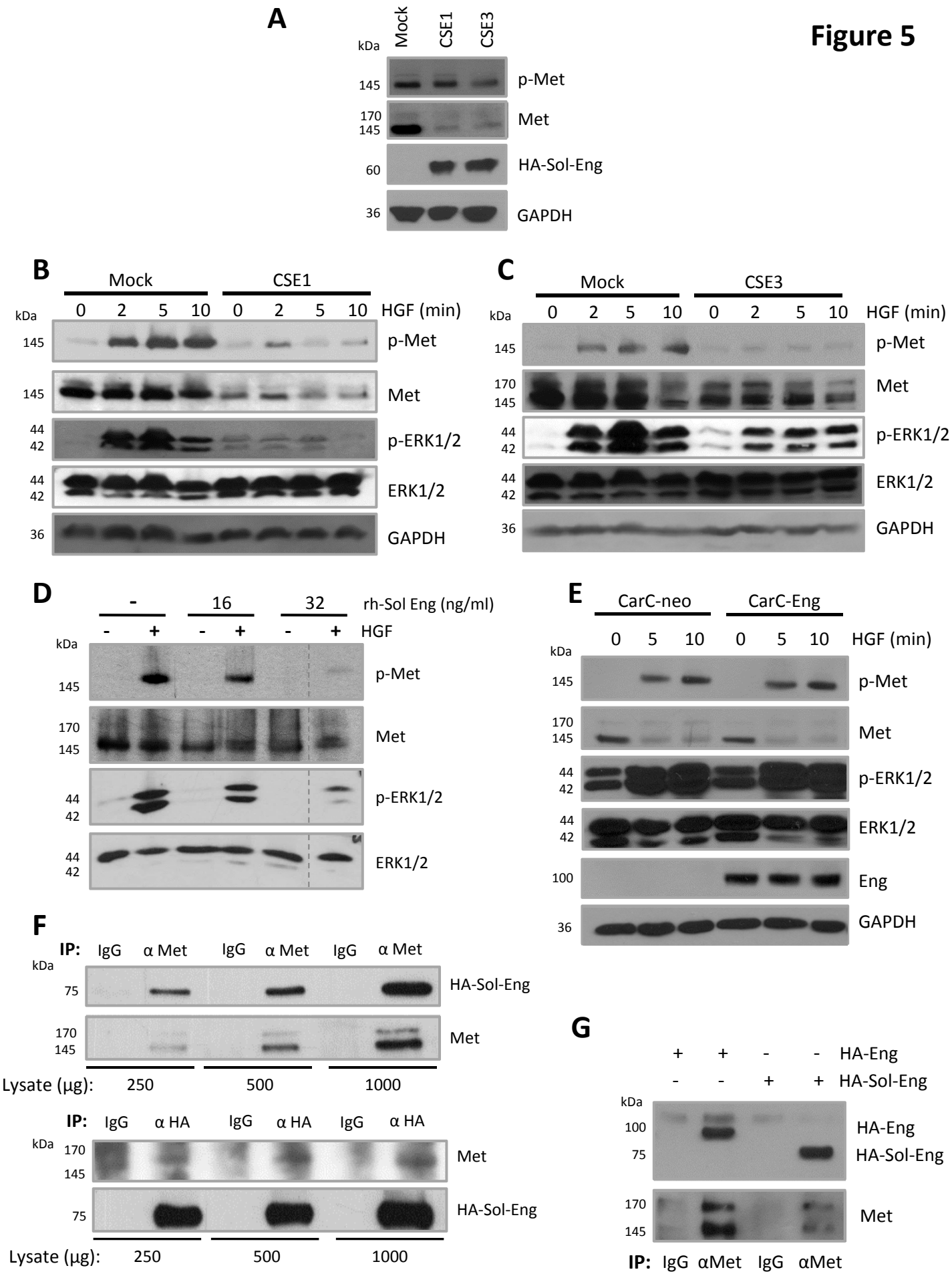
A
Mock
CSE1
CSE3
kDa
145
p-Met
170
145
Met
60
HA-Sol-Eng
36
GAPDH
B
Mock
CSE1
0 2 5 10 0 2 5 10 HGF (min)
kDa
145
p-Met
145
Met
44
42
p-ERK1/2
44
42
ERK1/2
36
GAPDH
C
Mock
CSE3
0 2 5 10 0 2 5 10 HGF (min)
kDa
145
p-Met
170
145
Met
44
42
p-ERK1/2
44
42
ERK1/2
36
GAPDH
D
- 16 32 rh-Sol Eng (ng/ml)
- + - + - + HGF
kDa
145
p-Met
170
145
Met
44
42
p-ERK1/2
44
42
ERK1/2
E
CarC-neo
CarC-Eng
0 5 10 0 5 10 HGF (min)
kDa
145
p-Met
170
145
Met
44
42
p-ERK1/2
44
42
ERK1/2
100
Eng
36
GAPDH
F
IP: IgG α Met IgG α Met IgG α Met
kDa
75
HA-Sol-Eng
170
145
Met
Lysate (µg): 250 500 1000
IP: IgG α HA IgG α HA IgG α HA
kDa
170
145
Met
75
HA-Sol-Eng
Lysate (µg): 250 500 1000
G
+ + - - HA-Eng
- - + + HA-Sol-Eng
kDa
100
HA-Eng
75
HA-Sol-Eng
170
145
Met
IP: IgG αMet IgG αMet

# Figure 6

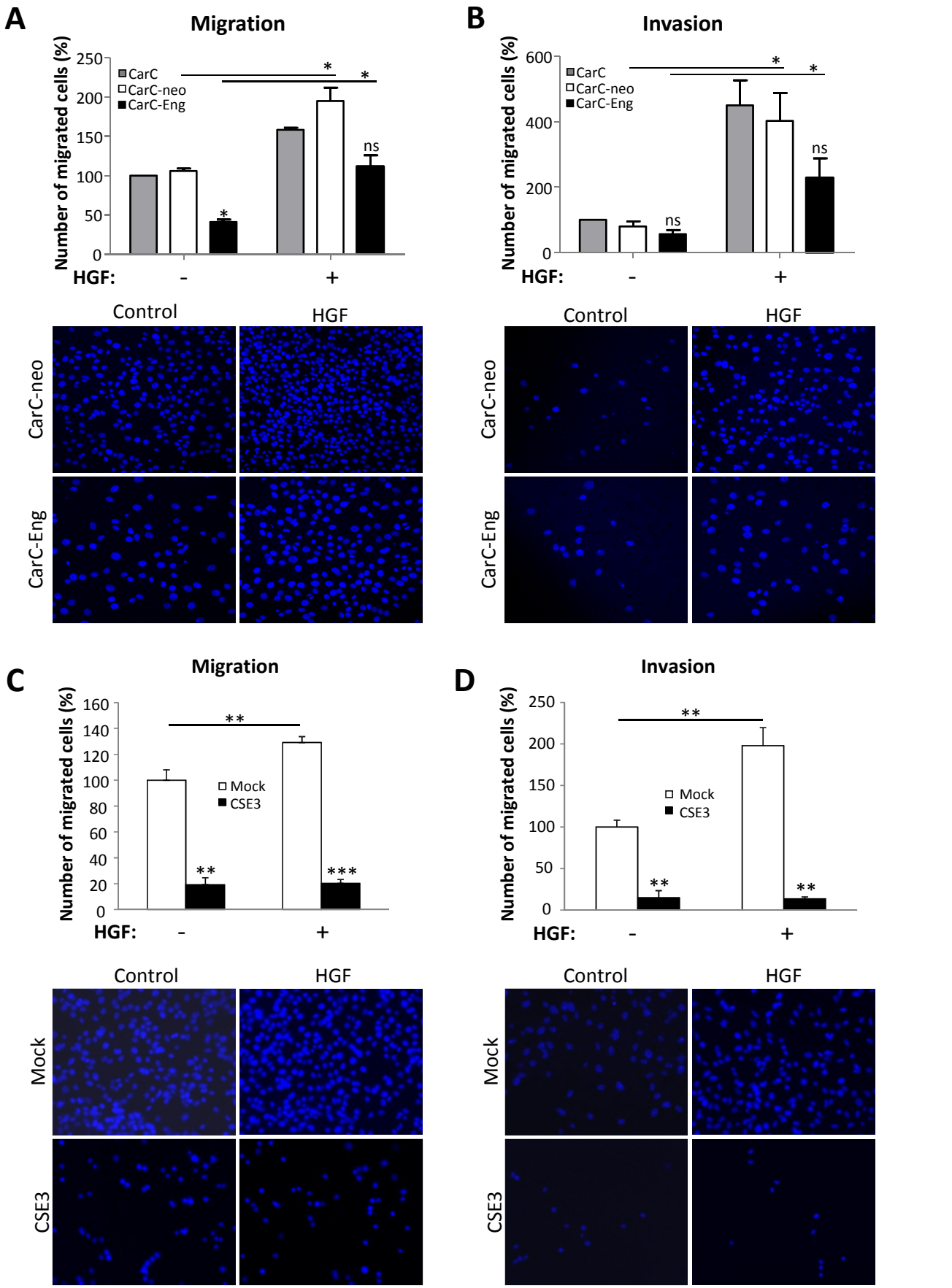
A
Migration
Number of migrated cells (%)
CarC
CarC-neo
CarC-Eng
HGF:
Control
HGF
CarC-neo
CarC-Eng
B
Invasion
Number of migrated cells (%)
CarC
CarC-neo
CarC-Eng
HGF:
Control
HGF
CarC-neo
CarC-Eng
C
Migration
Number of migrated cells (%)
Mock
CSE3
HGF:
Control
HGF
Mock
CSE3
D
Invasion
Number of migrated cells (%)
Mock
CSE3
HGF:
Control
HGF
Mock
CSE3

# Supplementary Figure 1

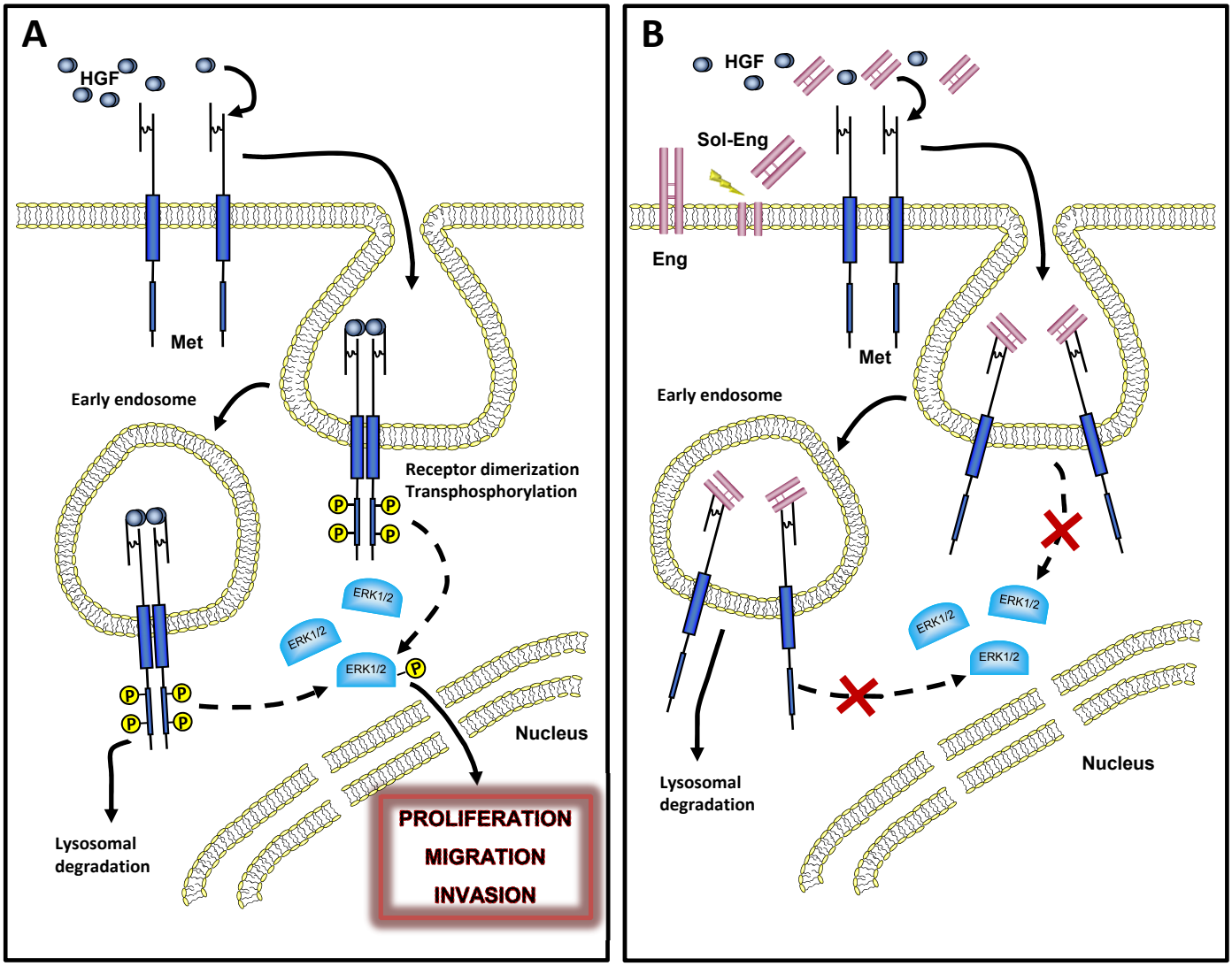

# Figure E